JOURNAL OF THE MECHANICAL BEHAVIOR OF BIOMEDICAL MATERIALS 28 (2013) 354–365

Available online at www.sciencedirect.com

ScienceDirect

www.elsevier.com/locate/jmbbm

Research Paper

Mechanically tissue-like elastomeric polymers and their potential as a vehicle to deliver functional cardiomyocytes

Bing Xu[a], *Yuan Li*[a], *Xiya Fang*[a], *George A. Thouas*[b], *Wayne D. Cook*[a], *Donald F. Newgreen*[c], *Qizhi Chen*[a,*]

[a]*Department of Materials Engineering and Monash Centre of Electron Microscope, Monash University, Clayton, Victoria 3800, Australia*

[b]*Department of Zoology, The University of Melbourne, Parkville, Victoria 3010, Australia*

[c]*Murdoch Childrens Research Institute, The Royal Children's hospital, Flemington Road, Parkville, Victoria 3052, Australia*

ARTICLE INFO

Article history:
Received 20 March 2013
Received in revised form
30 May 2013
Accepted 13 June 2013
Available online 21 June 2013

Keywords:
Elastomer
Poly(glycerol sebacate) fibre
Core/shell electrospinning
Cardiomyocyte

ABSTRACT

One of the major challenges in the field of biomaterials engineering is the replication of the non-linear elasticity observed in soft tissues. In the present study, non-linearly elastic biomaterials were successfully fabricated from a chemically cross-linked elastomeric poly (glycerol sebacate) (PGS) and thermoplastic poly(L-lactic acid) (PLLA) using the core/shell electrospinning technique. The spun fibrous materials, containing a PGS core and PLLA shell, demonstrated J-shaped stress–strain curves, and having ultimate tensile strength, rupture elongation, and stiffness constants respectively comparable to muscle tissue properties. *In vitro* evaluations also showed that PGS/PLLA fibrous biomaterials possess excellent biocompatibility, capable of supporting human stem-cell-derived cardiomyocytes over several weeks in culture. Therefore, the core/shell electrospun elastomeric materials provide a new potential scaffold to support cells in the therapy of a wide range of soft tissues exposed to cyclic deformation, such as tendon, ligament, cardiac or smooth muscle and lung epithelium.

1. Introduction

The stress–strain nature of biological tissues has been observed by several/many workers (Mirsky, 1976) to be quite unlike most materials. They undergo elastic (i.e, reversible) stretching to high levels of extensibility but they also exhibit non-linear deformation behaviour in which the stress rises at an increasing rate as the strain is raised. In contrast, thermoplastic polymers proposed for tissue replacement, such as polylactic acid (PLA), polyglycolic acid (PGA) and their copolymers, show a decreasing rate of rise in stress prior to plastic deformation (i.e. non-reversible deformation) at low strains. Therefore, one of the major problems encountered by biomaterials scientists in repairing the majority of soft tissue types is the need to replicate this innate and complex elasticity (Chen et al., 2008b). Despite some previous success (Seal et al., 2001), there are few synthetic tissue engineering products available for clinical use (Freed et al., 2009) in the

*Corresponding author. Tel.: +61 3 9905 3599; fax: +61 3 9905 4940.
E-mail addresses: qizhi.chen@monash.edu, qzchen202@gmail.com (Q. Chen).

1751-6161
http://dx.doi.org/10.1016/j.jmbbm.2013.06.005

repair of soft, mechanically functional tissues, such as heart, lung and intestine. These mechanical dissimilarities between synthetic biomaterials and tissue for repair are believed to be the major cause of graft failure in experimental animal studies and preclinical trials (Freed et al., 2006).

Research activity focusing on the development and clinical application of synthetic biodegradable soft elastomers as transplantable biomaterials for tissue engineering has increased over the past decade (Chen et al., 2008b). For example, poly (polyol sebacate; PPS) is a new family of cross-linked, biodegradable elastomers that has recently been developed for soft tissue repair and regeneration applications (Bettinger et al., 2006; Wang et al., 2002). Chen et al., 2008a,b have reported that the Young's modulus of a PPS family member, poly(glycerol sebacate; PGS), ranges between 0.05 and 1.5 MPa, which is similar to the stiffness of muscle tissues (Chen et al., 2008a).

In an animal study using a rat model, PGS sheets were grafted as heart patches and performed the intended mechanical function in terms of inhibiting scar formation in infracted heart muscles (Stuckey et al., 2010). However, this study also revealed two critical drawbacks of using PGS patches. Firstly, the grafted patches were completely absorbed in 6 weeks. This time frame is too rapid for the recovery of a diseased heart, a process which takes approximately 6–12 months (Stuckey et al., 2010). Secondly, and perhaps more significantly, an arrhythmia (irregular heartbeat), attributable to the mechanical property mismatch between the PGS patch and the heart muscle, was observed. The stress–strain curves of synthetic elastomers are relatively *linear* at low strains, particularly at 15% which is the maximal strain of living tissues, but biological tissues, such as heart muscles, exhibit *non-linear* stress–strain curves (Chen et al., 2008b) which we call here "J-shaped" as discussed above. The primary reason for these different elastic behaviours may be that the polymer chains form random coils between the crosslink points within the synthetic elastomer network, while protein nanofibres tend to be straighter and aligned within muscle fibres. Therefore, the production of an aligned, or partially aligned, nanofibrous structure within a synthetic polymer may be ideal for matching the non-linear elasticity of biological tissues.

The production of nanofibres from cross-linked elastomers is technically challenging. The first challenge of producing synthetic core–shell nanofibres has been recently solved by electrospinning (Jiang et al., 2006; Sun et al., 2003; Zhang et al., 2004). A second problem is that a crosslinked elastomer cannot be dissolved in a solvent for the electrospinning process. While the literature reports studies on photopolymerization of monomers and oligomers during the electrospinning process (Anseth et al., 1999), such a technique is not possible with the PPS materials of interest here because they contain no photopolymerizable groups. If the material is not photopolymerized during electrospinning, it must be capable of forming a rigid, relatively non-adhesive fibre once the solvent has evaporated. However before thermal crosslinking of PPS it is a viscous polymer which could not retain a nanofibrous form after spinning. In fact the PPS oligomer needs to be thermally cured at elevated temperatures to form an elastomer. Fortunately, the recent development of a core/shell electrospinning technique could offer an opportunity to address these problems (Ou et al., 2011; Ravichandran et al., 2011; Yi and Lavan, 2008). Core/shell electro-spun fibres are formed when a pre-polymer that is not cross-linked is en-sheathed by a suitable thermoplastic in solution, with both materials being fed into the electrospinner simultaneously but via separate core and annulus flows. Following collection of the core–shell nano-fibre, thermal crosslinking process of the prepolymer can be undertaken in situ if the solid thermoplastic shell can maintain its tubular shape at the curing temperature. Yi and Lavan (2008) have reported the production of core–shell PGS/ poly-L-lactic acid (PLLA) nanofibres using this method. In addition, they claimed that they could remove the thermoplastic shell from the final product by dissolution in chloroform. However, we believe that, when used as a biomaterial scaffold, the addition of a thermoplastic shell would be beneficial in controlling the degradation rate of the final product. Therefore, the objective of the present study was to systematically explore the fabrication procedures of PGS/PLLA fibrous materials using the core/shell electrospinning technique, to investigate the mechanical behaviour of these mats, and evaluate their *in vitro* biocompatibility as biomaterial scaffolds.

2. Experimental procedures

2.1. Materials

Glycerol, sebacic acid, L(+)-lactic acid (LA) were purchased from Sigma-Aldrich (Castle Hill, NSW, AU). Chloroform, dimethylformamide (DMF) and tetrahydrofuran (THF) were purchased from Merck (Kilsyth, VIC, AU). The PLLA, also known as RESOMER® L 206S, was purchased from Sigma-Aldrich (Castle Hill, NSW, AU) and is reported to be ester-terminated with an inherent viscosity of 0.8–1.2 dl/g for a 0.1% solution in $CHCl_3$ at 25 °C, a glass transition temperature of 60–65° and a melting point of 180–185 °C [http://www.sigmaaldrich.com/materials-science/polymer-science/resomer.html]. This PLLA was chosen as the shell material because its melting point is sufficient to retain the nano-fibre shape during the cross-linking of PGS, at tem peratures which range from 120 to 150 °C (Chen et al., 2010d, 2011; Liang et al., 2010).

PLLA has been successfully spun from a mixture of dichloromethane and DMF at volume ratios of 9:1 by Ou et al. (2011) but we did not find this system to be successful due to the rapid evaporation of the dichloromethane. Substitution of dichloromethane by the higher boiling chloroform at differing solvent ratios revealed the 4:1 v/v of chloroform to DMF to be the most successful. So it was selected as the solvent for the PGS prepolymer. THF has been used as a solvent for the casting of PGS pre-polymers in our laboratory and so preliminary studies with PGS pre-polymer concentrations from 10% to 50% w/v in THF were used in core–shell electrospinning but solutions spun with 50% w/v were found to give the best results.

2.2. PGS/PLLA solution miscibility and preparation of PGS-PLLA blends

In the core/shell electrospinning process, the core (PGS) and shell (PLLA) solutions are extruded from two concentric syringe needles and are spun together, thus remaining in intimate contact during the process. An essential requirement for a

successful core–shell spinning process is that these two solutions are not particularly miscible when they are in contact, so that the shell structure can be maintained during the spinning processes and during the subsequent thermal curing treatment. Therefore studies were undertaken of the miscibility of the solutions.

The PLLA solution was added to the PGS pre-polymer solution at four different PLLA/(PLLA+PGS) percentages of 2, 5, 10 and 30 wt%. The miscibility was then determined by visually examining the precipitation of PLLA upon mixing. Conversely, the PGS pre-polymer solution was added to the PLLA solution at four different PGS/(PLLA+PGS) weight percentages of 2, 5, 10 and 30 wt%. The miscibility was then determined by visually examining the development of a layer of separate PGS solution on top of the PLLA solution.

To synthesise the PGS-PLLA blends, the PGS pre-polymer (50% w/v in THF), and PLLA (20% w/v, in 4:1 chloroform/DMF) were again prepared as above, then mixed to give four different PLLA/(PLLA+PGS) weight percentages of 2, 5, 10 and 30. After vigorous mixing the mixture phase separated into a clear PGS-rich top layer and a clear PLLA-rich bottom layer. In each case, the clear PGS-rich top layer was then cast onto a glass slide and dried overnight at room temperature and then cured under the same conditions as used for PGS (130 °C under a vacuum for 3 days). After curing, the polymer-blend layer was peeled from the substrate as discussed above and mechanically tested. Since the PLLA solution was not completely miscible with the PGS solution, the weight percentages are termed "nominal".

2.3. Synthesis of PGS-co-LA polymers

During the cross-linking treatment of core/shell spun fibres, it is possible for physical mixing (via diffusion) and a chemical reaction (via copolymerisation) to occur between the PGS pre-polymer and PLLA at the interface of their solutions. Therefore, it is important to examine the effects that polymer blending and copolymerisation exert on the elastic properties of the newly synthesised material.

To investigate the effect of copolymerisation, a series of PGS-co-LA polymers were synthesised for investigation. Glycerol and sebacic acid were thoroughly mixed in glass beakers at a glycerol: sebacate (G:S) molar ratio of either 1:1 or 2:3. These mixtures were then heat-treated at 130 °C under a nitrogenous atmosphere for 24 h, as described previously (Li et al., 2013), and a PGS pre-polymer was formed after cooling under nitrogen. PGS pre-polymers were then thoroughly mixed in lactic acid (L) at a G:S:L molar ratio of 1:1:(0.25, 0.5 or 1) or 2:3:(0.25, 0.5 or 1). These mixtures were then dissolved in THF, cast onto glass slides, dried under ambient conditions overnight, and then dried a second time under a vacuum overnight. The dried slides were then heated at 130 °C under a vacuum for 3 days to stimulate copolymerisation, followed by cooling to room temperature under a vacuum. Finally, the polymer sheets formed in this manner were peeled off after soaking in water, and thoroughly dried under a vacuum for 4 days at room temperature and then mechanically tested.

2.4. Core/shell electrospinning

A Y-Flow 2.2D-350 electrospinner (Yflow Nanotechnology Solutions, Spain) was set up with a two-fluid coaxial spinneret, and the inner tube had inner and outer tube diameters of 0.6 mm and 0.9 mm respectively while the outer tube had an inner diameter of 1.4 mm. Thus the cross-sectional areas of the two flows were 0.283 and 0.903 mm^2. A voltage potential ranging from 10 to 13 kV, but usually at 12 kV, was applied between the tip of the spinneret and the collector plate located 200 mm below. The feed flow rates of the core (50% w/v PGS in THF) and the shell (PLLA as a 20% w/v solution in a 4:1 chloroform/DMF) solutions ranged from 0.1 ml/h vs. 1 ml/h. The spun fibres were collected on a static plate and the spun fibre mats were then heated at 130 °C under vacuum for 3 days to cross-link the PGS.

2.5. Tensile testing

Tensile test specimens were punched out using a standard dog-bone-shaped mould, with a gauge length of 12.5 mm and a width of 3.25 mm. The thickness of each specimen was measured using a pair of callipers. Cyclic and tensile testing were conducted for each specimen at room temperature, using an Instron 5860 mechanical tester equipped with a 100 N load cell. All the testing data are expressed as true stress and strain – these were calculated from the engineering stress and strain assuming a Poisson ratio of 0.4 which is typical for polymeric materials. The cyclic test specimens were stretched to a maximum strain of 15% (1.88 mm), typical of the dynamic loading strain of soft tissues, such as cardiac muscle, under normal physiological conditions (Veress et al., 2005). The crosshead speed for cyclic testing was chosen to be 25 mm/min to enable comparison with previous studies (Lv et al., 2010). For the tensile tests, the crosshead speed was selected to be 10 mm/min which is also consistent with the rates used previously (Liang et al., 2010).

As these polymers are in a rubbery state, their true stress (σ)–strain (ε) behaviour can be readily described by the equation of rubber elasticity (Flory, 1953). At low strain values, this equation can be linearised with an error of 8.8% when $\varepsilon = 10\%$. For a material that obeys Hooke's law (i.e. the stress–strain relationship is linear), the Young's modulus E is defined by

$$E = \sigma/\varepsilon. \quad (1)$$

Therefore, the Young's modulus of each specimen was determined by taking the value of σ/ε when $\varepsilon = 10\%$. The ultimate tensile strength (UTS) and the elongation at the breaking values were read directly at the breaking point of the tensile test.

Resilience describes the capability of a material to deform reversibly without a loss of energy (Lv et al., 2010), and was calculated from the stress–strain data of the cyclic tests. The resilience of a material is expressed as the following ratio, for a strain of 15% (Bellingham et al., 2003):

$$\text{Resilience}\ (\%) = \frac{\text{area under unloading curve}}{\text{area under loading curve}} \quad (2)$$

Biological tissues are usually found to exhibit a non-linear elasticity and several constitutive equations have been proposed for this behaviour (Fung, 1967; Haut and Little, 1972; Mirsky, 1976; Stromber and Wiederhi, 1969). These functions predict that stress increases near-exponentially with strain.

Young's modulus is often replaced by the tangent modulus (also known as "stiffness" in medical science), defined as the slope at any point of a stress–strain curve. According to the equation of Mirsky et al. (Mirsky, 1976; Mirsky et al., 1974; Mirsky and Parmley, 1973), the tangent modulus, E, is proportional to the stress exerted on it, as in the following equation:

$$E = \frac{d\sigma_T}{d\varepsilon_T} = k\sigma_T + \alpha, \tag{3}$$

where the slope k (dimensionless) is defined as the stiffness constant. If the strain is low, the constant α is the Young's modulus. The derivative was determined at each point by linear regression of the five data values before and after that point. Several other workers (Fester and Samet, 1974; Takaoka et al., 2002) have also found that Eq. (3) provides a good model for biological tissues. In the present study, the stiffness constants of spun fibrous sheets were determined from the stress–strain curves of tensile specimens using Eq. (3).

2.6. Scanning electron microscopy

The surfaces of the fibre meshes were sputter-coated with platinum with ≈1 nm and characterised using a JEOL 7001F field emission gun scanning electron microscope (SEM), which was operated in second electron imaging mode. To observe the core/shell structure, fibre meshes were cut crosswise using an Ultracut S Cryo-Microtome at −120 °C. The cross-sections were also coated with platinum with ≈1 nm and then analysed by SEM.

2.7. Cytocompatibility assay

Cytocompatibility assays were performed according to the standard cytotoxicity assessment set by the International Standardization Organization (ISO 10993). Prior to culture, 48-well plates (Falcon, BD Bioscience, North Ryde, Australia) were coated with a 0.1% w/v gelatine solution and washed using phosphate-buffered saline to remove any residual solvent. SNL Mouse fibroblasts (STO-Neo-LIF, University of California, Davis) were then seeded to each well, which contained 1 ml of Dulbecco's modified Eagle's medium (DMEM) (Gibco®, Australia) supplemented with 10.0% foetal bovine serum, 1.0% Glutamax(Gibco®, Australia), and 0.5% penicillin/streptomycin, at a target density of 5000 cells/well. The negative control for the test was 1 ml of the cell culture media with no additives. The PLLA-only fibre meshes were used as a material control, and the cell culture medium containing inoculated cells without scaffolds was used as a positive control. The plate was then cultured under standard incubation conditions of 37 °C and 5% CO_2 in humid air, with medium changed every second day. When cell monolayer had reached a confluence of 80% on day 4, electro-spun PGS/PLLA core/shell fibre mats and control PLLA fibre mats (sterilised by treatment with 70% ethanol in deionised water, and dried overnight in a cell culture hood) were placed in contact with the cell monolayer covered with cell culture medium in the 48-well plate. Cultures were then allowed to grow for a further 2 days, as we have done in a previous study (Liang et al., 2012).

At the end of the incubation period, the spent culture media samples were collected and the degree of cytotoxicity was determined using a commercial assay kit (TOX-7, Sigma-Aldrich) (Chen et al., 2010c; Liang et al., 2010) to measure the quantity of lactate dehydrogenase (LDH) released into the culture media by dead or dying cells ('dead LDH'). Wells with live cells were then filled with 0.5 ml of fresh cell culture medium containing TOX-7 lysis buffer, and cellular LDH was then extracted from these lysates ('live LDH'). The overall LDH level per well was then determined by measuring the absorbance of the supernatant from the centrifuged medium at 490 nm (after subtracting the background absorbance at 690 nm), using a multi-well plate UV–vis spectrophotometer (Thermo Scientific). The LDH absorbances were converted to a cell count based on a linear standard curve. Therefore, the cytotoxicity can be expressed as follows:

$$\text{Percentage of dead cells} = \frac{\text{dead LDH}}{\text{dead LDH} + \text{live LDH}} \times 100. \tag{4}$$

2.8. Cell proliferation

Cell proliferation was assessed using a commercial AlamarBlue™ assay kit (Life Technologies). AlamarBlue™ is non-toxic to cells and does not interrupt cell culture growth, but AlamarBlue is reduced by living cells to the reduced form which has a different absorption spectrum in the visible region, allowing quantitative measurement of the cell activity and a continuous measurement of cell proliferation kinetics. Therefore, the AlamarBlue™ assay is appropriate for evaluating the long-term cytotoxicity of biomaterials that undergo biodegradation under physiological conditions (Chen et al., 2010b). For this assay, culture media wells were seeded with SNL fibroblasts (2000 cells per ml) into each well of a 48-well plate and cultured as described above, in the presence of sterilised PGS/PLLA fibre meshes (test material) or sterilised PLLA fibre meshes (material control). Material-free media with cells (positive controls) and the cell culture medium alone (negative control) were also included in independent wells on the same plate.

After culture for 48 h, 0.1 ml of the AlamarBlue™ indicator was added to each well (with the exception of the background controls) and incubated under standard culture conditions for a further 5 h. The medium was then transferred to a new plate, after which the UV–vis absorbance of the medium at wavelengths of 570–600 nm was measured. This procedure was repeated every 48 h until confluence was reached, which was typically after 6 days. Cell proliferation was quantified by the percentage reduction of AlamarBlue™ from its normal oxidised form to the reduced from using the following equation (Chen et al., 2010a):

$$\%\,\text{Reduced} = \frac{\varepsilon_{OX}(\lambda_2)A(\lambda_1) - \varepsilon_{OX}(\lambda_1)A(\lambda_2)}{\varepsilon_{RED}(\lambda_1)A'(\lambda_2) - \varepsilon_{RED}(\lambda_2)A'(\lambda_1)} \times 100. \tag{5}$$

where $A(\lambda_1)$ and $A(\lambda_2)$ are the absorbance values of test wells measured at wavelengths $\lambda_1 = 570$ nm and $\lambda_2 = 600$ nm, respectively, and $A'(\lambda_1)$ and $A'(\lambda_2)$ are the values of absorbance at the same wavelengths for negative control wells containing only culture medium and AlamarBlue™. All values were blanked based on the readings of background controls. The remaining

parameters were the molar extinction coefficients: $\varepsilon_{OX}(\lambda_1)=80.586$, $\varepsilon_{OX}(\lambda_2)=117.216$ for the oxidised form and $\varepsilon_{RED}(\lambda_1)=155.677$ and $\varepsilon_{RED}(\lambda_2)=14.652$ for the reduced form.

2.9. Viability of hESC-derived cardiomyocytes

hESC cell culturing and differentiation of the MIXL1GFP/w cell line, a hES3 derivative, were performed as previously described (Chen et al., 2010d). Briefly, differentiations used forced aggregation of hESCs in low adherent dishes in APEL media to form embryoid bodies (EBs). EBs were transferred to adherent dishes in BEL media at day 7 and recordings began at day 14 continuing every 2 days for a further 28 days. The contractile motion of the cells was studied through a Nikon Eclipse TS100 inverted microscope with Hoffman modulation contrast optics, coupled to a Basler (model A602f) camera and captured using Quick Caliper (SDR Clinical Technologies) software at 80 frames s^{-1}. The video captures were analysed using the Metamorph® Imaging software suite. The rationale for this approach is that (a) ESC-derived cardiomyocytes (ESC-CMs) have a strong tendency to aggregate so techniques to assessing cell viability and cytotoxicity based on the homogenous seeding density of cells cannot accurately be achieved; and (b) overgrowth with more rapidly proliferating fibroblasts may bias these methods. Therefore, we used the intrinsic contractile activity of cardiomyocytes and scored the beating rates of hESC-CMs by videomicroscopy.

2.10. Statistical analysis

All experiments were performed with five samples per experimental group, and the statistical outputs are shown in the form of a mean with standard error (± SE). A one-way analysis of variance (ANOVA) with Turkey's *post hoc* test was performed to analyse the significant differences, and significance levels were set at a p-value of less than 0.05.

3. Results and discussion

3.1. Miscibility of the PLLA and the PGS solutions

When the 20% w/v PLLA solution was added to the 50% w/v PGS solution, phase separation was observed in mixtures containing between 2 and 5 wt% of the PLLA solution. Therefore, the miscibility of the PLLA solution with the PGS solution is between 2 and 5 wt%. After small amounts of the 50% w/v PGS solution was added to the 20% w/v PLLA solution, phase separation was observed, indicating that the miscibility of the PGS solution in the PLLA solution is lower than 2 wt%. These results indicate that the PLLA and PGS solutions should largely remain in their separate phases during core/shell spinning. However, it remains possible that small amounts of the PLLA shell material will dissolve in the PGS core material and this may compromise the elastomer's properties. This small amount of PLLA may exist as an intimate solution with the PGS polymer chains, or it may also react with the PGS during cross-linking to form a PGS-co-LA polymer. Therefore, the effects of the presence of PLLA on the mechanical properties of the PGS/PLLA blends were investigated.

3.2. Mechanical properties of PGS/PLLA blends

The PGS/PLLA mixtures (either copolymers or blends or both) were prepared by adding PLLA to a PGS pre-polymer, cast into sheets and the solvent evaporated followed by heat treatment to cross-link the pre-polymer chains (Table 1). With an increase in the nominal wt% of PLLA, the Young's modulus, UTS, elongation at break and resilience do not change significantly (Table 1). The addition of the PLLA to the blend does not considerably compromise the elasticity of the PGS matrix (Table 1). It is interesting to note that the elongations at the break point of the PGS/PLLA blends were collectively, and on average, higher than pure PGS, although the increments were not statistically significant.

3.3. Mechanical properties of PGS-co-LA polymers

The mechanical properties of the PGS-co-LA polymers with a 1:1 or 2:3 M ratio of PGS to LA are shown in Table 2. Young's moduli and UTS values of the 1:1 PGS-co-LA polymer are similar to those of the pure PGS counterpart, and no significant differences were detected between any pair of the four polymer groups compared to each other. Two counteracting mechanisms could likely be responsible for the lack of significant changes. Lactic acid contains both hydroxyl and carboxyl groups and can therefore react with both glycerol and sebacic acid. Therefore lactate units in the network chains will increase the physical distance between the cross-link points, lowering density of cross-links and reducing the rubbery modulus and strength (Flory, 1953) in comparison with a pure PGS polymer that is treated under identical conditions. Furthermore, lactic acid should significantly reduce the polymerisation kinetics in comparison with the polymerisation of pure PGS. This observation was in accordance with experiments which show that the polycondensation reaction of lactic acid is much slower than that of glycerol and sebacate and requires a higher reaction temperature (Malberg et al., 2010; Sun et al., 2009). Therefore,

Table 1 – Mechanical properties of PGS/PLLA blend/copolymers after heat treatment in vacuum at 130 °C for three days to crosslink the PGS component.

Nominal percentage of PLLA in blends (wt%)	Young's modulus (MPa)	UTS (MPa)	Elongation at break (%)	Resilience
0	1.23±0.06	0.70±0.04	88±8	0.975±0.005
5	1.27±0.05	1.04±0.15	124±18	0.977±0.007
10	1.17±0.27	0.77±0.07	101±36	0.969±0.011
20	1.23±0.09	0.73±0.10	83±19	0.968±0.012

Table 2 – Mechanical properties of the PGS-co-LLA polymer synthesised with a 1:1 or 2:3 G:S molar ratio in a vacuum at 130 °C for three days.

	Molar ratio of glycerol: sebacic acid: lactic acid							
	1:1:0	1:1:0.25	1:1:0.5	1:1:1	2:3:0	2:3:0.25	2:3:0.5	2:3:1
Young's Modulus E (MPa)	1.03 ± 0.05	0.88 ± 0.07	0.99 ± 0.04	0.89 ± 0.02	1.59 ± 0.04	1.81 ± 0.16	1.81 ± 0.05	1.65 ± 0.04
UTS (MPa)	0.69 ± 0.04	1.05 ± 0.16	0.77 ± 0.08	0.74 ± 0.11	0.72 ± 0.03	0.88 ± 0.03	0.82 ± 0.09	0.94 ± 0.08
Elongation at break (%)	88.65 ± 8.36	110.96 ± 22.11	84.23 ± 11.05	125.38 ± 0.99	51.35 ± 2.01	61.92 ± 5.28	53.85 ± 6.53	69.23 ± 7.59
Resilience	0.96 ± 0.006	0.97 ± 0.002	0.97 ± 0.006	0.97 ± 0.004	0.97 ± 0.002	0.97 ± 0.005	0.97 ± 0.003	0.98 ± 0.003

the incorporation of lactic acid into the PGS network has a tendency to soften the polymer product because it reduces the extent of polyesterification compared with that in neat PGS. Conversely, the side $–CH_3$ chains on lactic acid molecules could stiffen the copolymer network by increasing its T_g, since PLLA has a T_g of 60–65 °C [http://www.sigmaaldrich.com/materials-science/polymer-science/resomer.html] compared with −23 °C for PGS (Liang et al., 2012). In this manner, these counteracting mechanisms could result in relatively insignif icant changes to the Young's modulus and to the UTS in the PGS-co-LA polymers, compared to pure PGS or PLLA.

The results of Table 2 also partly concur with those of Sun et al. with regard to poly(glycerol–sebacate–lactic acid) (Sun et al., 2009), where the copolymers were synthesised at 140 °C for 30 h and the elastic moduli of the copolymers were measured using nano-indentation. Their study showed no significant increments in the elastic moduli of the copolymers synthesised at a G:S:L molar ratio of 1:1:(0–0.5), as conducted in the present study. However, the elastic modulus of the copolymer increased abruptly at a molar ratio of 1:1:1 (Sun et al., 2009), which was inconsistent with our result for the same ratio. This discrepancy is likely caused by the different synthesis conditions used in forming the copolymer, or in the different testing methods used (surface versus bulk). Further research is required to enable an in-depth understanding of the effects of treatment temperature on the cross-linking kinetics and surface structure of the PGS-co-LA system.

The elongation at the breaking point and the resilience of the PGS-co-LA polymers were similar to those for the pure PGS polymer, and there were no statistical differences between any pair of the four PGS-based polymers containing a 1:1 or 2:3 G:S molar ratio. This indicates that even if PGS-co-LA had formed copolymers along the interface of a core and shell fibre, the elastic properties of the core PGS fibres would not be compromised, and PGS-co-LA copolymers could also be spun as the core of a fibrous material.

A comparison of the PGS-based polymers at a 1:1 and 2:3 M ratio shows that the former had approximately two thirds of Young's moduli (approximately 1 MPa), and almost double the elongation at rupture (80–120%) compared to the PGS-based materials containing 2:3 G:S molar ratios (1.5 MPa and 50–70%, respectively). There are three hydroxyl groups in a glycerol monomer and two carboxyl groups in a sebacic acid monomer. The reaction kinetics of the primary –OH groups, which is found at both terminals of the glycerol molecule, are faster than those of the secondary –OH groups found in the middle of the glycerol molecule (Li et al., 2013) at a temperature of 100–150 °C, such that the polymerisation is dominated by the formation of PGS polymer chains. The cross-linking process through reaction of the secondary –OH groups, becomes the dominant kinetic process only when the free primary –OH groups in the reactant system have been consumed. At a 1:1 G:S molar ratio, esterification is dominated by the reaction of the primary hydroxyl groups with sebacic acid, leaving a large fraction of the secondary –OH groups on the glycerol units unreacted, thus lowering the cross-link density of the PGS network. At a 2:3 G:S molar ratio, which is the theoretical stoichiometric molar ratio required for a complete reaction between the hydroxyl and the

carboxyl groups, most of the secondary –OH groups are reacted, resulting in a highly cross-linked network. As a result of the higher crosslink density of the systems with the 2:3 G:S molar ratio, the modulus is higher and the elongation to break lower.

Table 2 shows high resilience of these polymers and no significant effect of crosslinking on the UTS. Depending on the crosslink density, the UTS can either increase or decrease as the crosslink density rises (Taylor and Darin, 1955) as a result of competing factors. Thus it appears that for the systems with 1:1 and 2:3 G:S molar ratios, the crosslink densities are close to the maximum in the dependence of UTS on crosslinking.

Based on the desirable elongation to break, the PGS formed by a 1:1 G:S molar ratio was considered to be the best choice for use in the present study.

3.4. *Optimisation of the core/shell electrospinning conditions*

The parameters that affect electrospinning and the resultant PLLA polymer fibres that are spun have been extensively described in the relevant literature (Bognitzki et al., 2001; Caruso R.A., 2001; Tsuji et al., 2006), including PLLA solution parameters (such as the molecular weight and the surface tension) and the processing conditions, including the electrical potential, operating temperature and feed flow rates. The most important factor affecting the core/shell spinning process in the present study was the ratio of the feed flow rate of the core solution to that of the shell solution. Polymer globules were formed in the fibre meshes (Fig. 1a) when the feed flow rate of the PGS core solution (0.1 mL/h) was 20 times lower than that of the shell solution (2.0 mL/h). The globules formed in the present core/shell spun meshes, as shown in Fig. 1a, were approximately 10 μm in diameter and these were larger and more spherical than the 1 μm globules which have been observed by other researcher (Li and Xia, 2004) in the electro-spinning of fibrous PLLA mats. Li and Xia (2004)) have suggested that globules or beads are formed on the electropsun fibres as a competition between the entanglement-controlled viscoelastic properties of the polymer solution(s) which tends to form fibres, the surface tension effect which tends to form droplets and the electrostatic forces which tend to increase the surface area and thus form fibres. They also suggested that the formation of beads can be eliminated by increasing the polymer concentration, however in our work variation of the concentrations of the core and the shell solutions failed to prevent the formation of the globules. Thus polymer concentration may not be the only factor affecting bead formation. When we increased the feed flow rate of the core PGS solution, the formation of the large beads was effectively eliminated and we produced fibres with uniform diameter (Fig. 1b and c). Thus when low feed flow rates of the core are used (e.g. 0.10 mL/h for core and 2 ml/h for shell as in Fig. 1a) the core solution may not be able to maintain a continuous flow, therefore causing an accumulation of the core solution around the inner needle tip, which periodically collapses into the shell after the core accumulation had reached a certain level. The morphology in Fig. 1b resulted from slower core versus shell solution feed rates

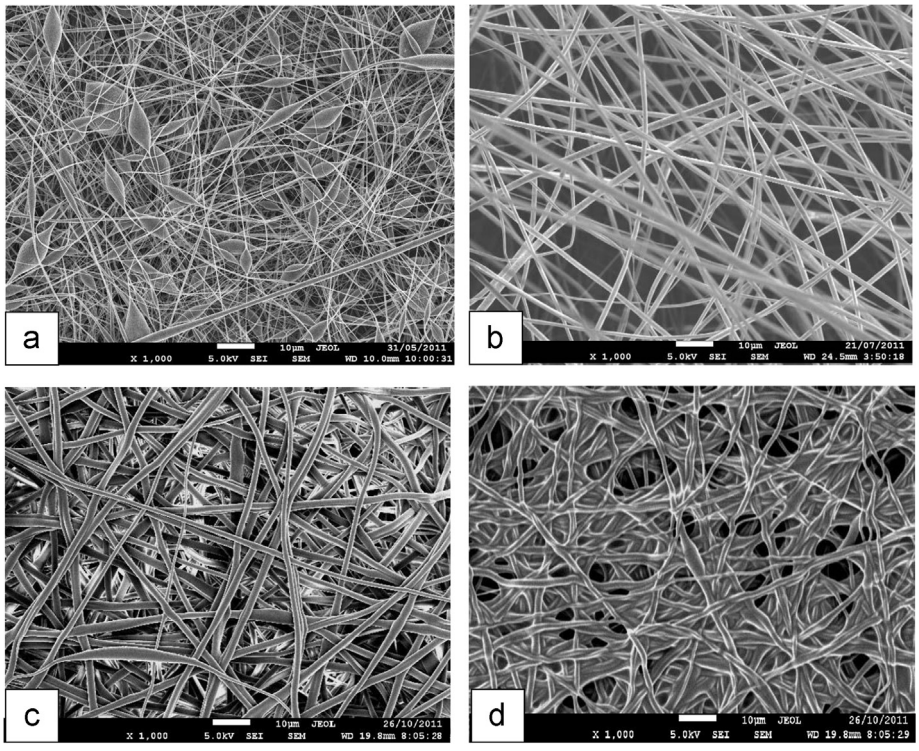

Fig. 1 – SEM images of PGS/PLLA core/shell fibres fabricated at different core to shell feed flow rates: 0.10 ml/h vs. 2 ml/h at 10 kV (a), 0.20 ml/h vs. 0.80 ml/h at 12 kV (b), 0.30 ml/h vs. 0.90 ml/h at 12 kV (c) and 0.50 ml/h vs. 1.0 ml/h at 13 kV (d). The material was heat treated for crosslinking at 130 °C for three days. The optimal conditions are (b) and (c). The ratios of core solution radius and shell solution thickness in spinning (by theoretic calculation) for (a)–(d) are 0.28, 0.81, 1.00 and 1.37.

(0.2 ml/h vs. 0.80 ml/h), similar to Fig. 1c (0.30 vs. 0.90 ml/h). However, when these were increased (0.50 vs. 1.0 ml/h), the fibres became fused to each other (Fig. 1d). It appears that at the latter high feed rates (0.50 vs. 1.0 ml/h), the amount of shell material being fed into the spinneret was insufficient to fully cover the core, leading to the leakage of the PGS pre-polymer, which resulted in a fusion of the fibres when they were heat-treated for cross-linking.

For the examination of the core/shell structure, a fibre mesh was sectioned in liquid nitrogen, using the cryogenic microtome sectioning technique, and the cross section was examined by SEM. Fig. 2 shows an example of the PGS/PLLA core/shell fibrous mats produced at one of the optimal conditions (Table 3), while Fig. 3 shows that a nano-porous structure was observed in the PLLA shell throughout the fibrous sample, which is in accordance with the results of previous studies (Bognitzki et al., 2001; Caruso and Greiner, 2001; Tsuji et al., 2006). The formation of porosity is probably the result of the evaporation of THF from the spun PLLA/THF core solution. An additional benefit of this nano-porous structure is that it softens the rigid PLLA shell and so enhances the elastic match between the core PGS and shell PLLA under mechanical loading.

Table 4 shows that the fibre diameter increases as the core feeding rate is raised and the shell feeding rate is reduced. This does not appear to be due to the concentration of polymer in the solvents since these only vary from 25 to 27.5 wt% and so the reason for this variation in fibre diameter is uncertain.

In the study by Yi and Lavan (2008) of PGS/PLLA core/shell nanofibres, the final shell product was essentially a protective coating, and was ultimately removed, however we believe that maintenance of the PLLA shell can address the drawbacks of rapid PGS degradation. Firstly, the more slowly degrading PLLA shell can stabilise the degradation rate of the final product. Therefore, the composite material could be applied to the engineering of many types of soft tissues, which require long recovery periods of several months or years, and variable degradation kinetics. Secondly, the excellent biocompatibility of PLLA can improve the cytocompatibility of the fibrous mats, in comparison with the pure PGS fibres alone. Therefore, in this work the PLLA shell was retained in the final products, and the characterisation and bio-assessment was conducted on the PGS/PLLA core/shell fibrous materials as a composite scaffold.

3.5. *Mechanical properties of fibrous mesh materials*

The stress–strain curves of the PGS/PLLA core/shell fibrous sheet materials were J-shaped (Fig. 4), similar to the non-linear profile observed for biological tissue elasticity. The fractions of the more rigid PLLA and of the softer PGS in the fibres, the porosity of the mats and the adhesion of the fibres to one another are expected to have a large effect on the mechanical properties of the mats. Table 4 shows that the

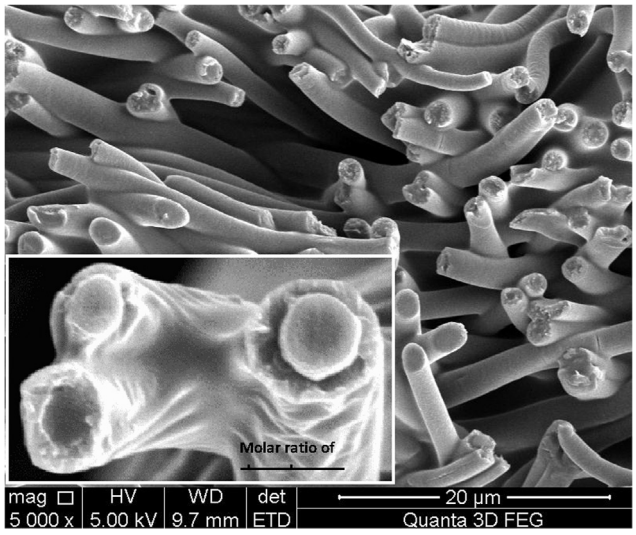

Fig. 2 – Cross-sectional SEM imaging of a PGS/PLLA core/shell fibrous sheet. The inset shows the core/shell structure at a high magnification. The fibres were spun at a core feed flow rate of 0.2 ml/h and a shell feed flow rate of 0.8 ml/h at 12 kV. The material was cross-linked at 130 °C for three days. The specimen was micro-sectioned in liquid nitrogen.

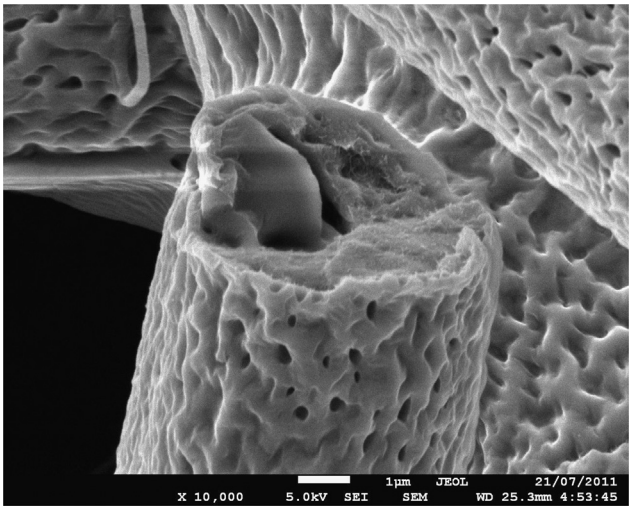

Fig. 3 – SEM image of the porous microstructure within the PLLA shell. The fibres were spun at a core feed flow rate of 0.2 ml/h and a shell feed flow rate of 0.8 ml/h at 12 kV. The material was cross-linked at 130 °C for three days. The specimen was sectioned at −120 °C.

Table 3 – Optimal core/shell electrospinning conditions under a voltage potential of 12 kV.

PGS-THF solution (w/v)	Chloroform:DMF solvent	PLLA-(CF:DMF) solution (w/v)	Feeding rates of PGS (core):PLLA (shell)	Relative flow rate (ml/h)
50%	4:1	20%	0.30: 0.90 or 0.20: 0.80	1:3 or 1:4

Table 4 – Mechanical properties of the core/shell mats.

Feeding rates of PGS (core):PLLA (shell)	PLLA in the fibres (wt%)	Fibre diameter (μm)	Stiffness constant	UTS (MPa)	Elongation to rupture (%)
0.20:1.00	67	1.3±0.4	6±2	0.8±0.4	15±3
0.20:0.80	62	2.0±0.2	10±3	1.5±0.5	22±2
0.30:0.90	55	2.2±0.2	18±2	1±0.2	25±3

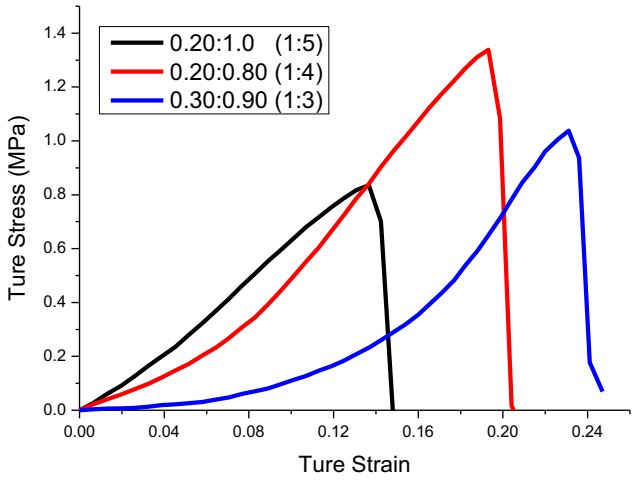

Fig. 4 – Stress–strain curves of the PGS (core)/PLLA (shell) fibre sheets fabricated at three cores to shell feed flow conditions: 0.2 ml/h to 1 ml/h, 0.2 ml/h to 0.8 ml/h and 0.3 ml/h vs. 0.9 ml/h.

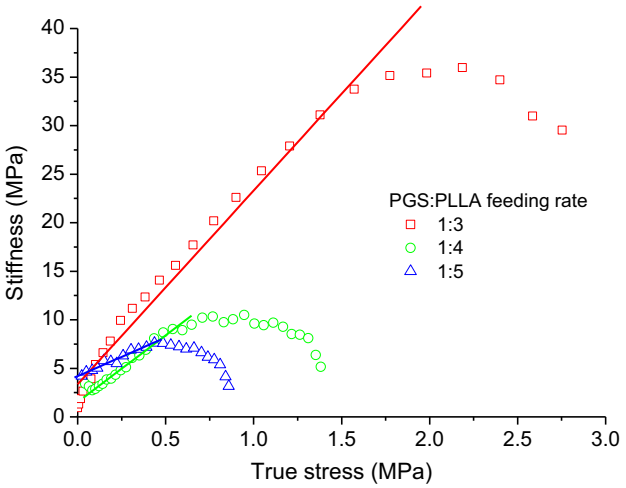

Fig. 5 – Stiffness–stress relationship of the PGS/PLA fibrous mesh material spun at different core/shell feeding rate 1:3. The stiffness constant of this stiffness–stress relationship is given in Table 4. For the 1:3 specimens the equation fitted the data up to 17±3%.

PLLA content in the fibres varies from 55% to 67% for the mats studied in Figs. 4 and 5. The fibrous mats varied in porosity from 73% to 76% w/v, based on the measurement of weight and volume of the spun mats. In addition, while the extent of fibre adhesion of one to another has not yet been determined, it is expected that this adhesion will significantly affect the stress–strain behaviour of the fibrous materials. However the main variation in behaviour of the mats in Figs. 4 and 5 appear to be due to the variation in the proportion of the more rigid PLLA shell to the more flexible PGS core. As a result, an increased core feed flow rate and thus a lower content of PLLA results in a more compliant and stretchable mesh having a larger elongation to rupture and a lower UTS, as given in Table 2.

Using the non-linear stress–strain equation proposed by Mirsky (Mirsky, 1976; Mirsky et al., 1974; Mirsky and Parmley, 1973) representative linear plots of stiffness versus stress are shown in Fig. 5. Only the system produced with a core feed flow rate of 0.3 ml/h and a shell feed flow rate of 0.9 ml/h were adequately fitted by Eq. 3, as indicated by the range of stress and strain that was fitted by the Equation. The UTS, elongation to break and stiffness constant of this system is 1.0±0.2 MPa, 25±3% and 18±2, respectively. The stiffness is (which are comparable to the values 12 to 20) previously exhibited by heart muscular tissues (Mirsky, 1976; Mirsky et al., 1974; Mirsky and Parmley, 1973) while the UTS and elongation to break are higher than the typical values of 0.02–0.5 MPa and 20% found for heart muscular tissues (Chen et al., 2008a; Chen et al., 2013).

The material produced at a core feed flow rate of 0.3 ml/h and a shell feed flow rate of 0.9 ml/h and containing 55 wt% PLLA was subjected to cyclic testing over five deformation and recovery cycles demonstrated that although the fibrous mesh material exhibited hysteresis and dissipated energy during the cycle, the stress–strain overlapped and were reproducible (Fig. 6). The resilience of these materials was determined to be ~70%, suggesting that they may be similar to elastomeric proteins, which have resilience ranges from 50% for partially hydrated elastin, to 90% for fully hydrated collagen and elastin (Gosline et al., 2002). The very flat segment is due to very low stress of fibrous sheet, typical feature of fibrous materials and soft tissue (Szczesny et al., 2012).

3.6. *In vitro evaluation: cellular viability and proliferation*

A visual examination of the SNL cell growth did not indicate major cytotoxicity in any of the tested groups, as shown in Fig. 7. SNL cells attached to the bottom well and proliferated in the material-free culture media and media soaked with PGS/PLLA and the PLLA fibrous materials. After 2 days, the number of cells in each well had increased to over 10,000 and almost covered the surfaces, as shown in Fig. 7. Quantitative measurements using the AlamarBlue™ reagent demonstrated that SNL cells proliferated almost linearly with time on the

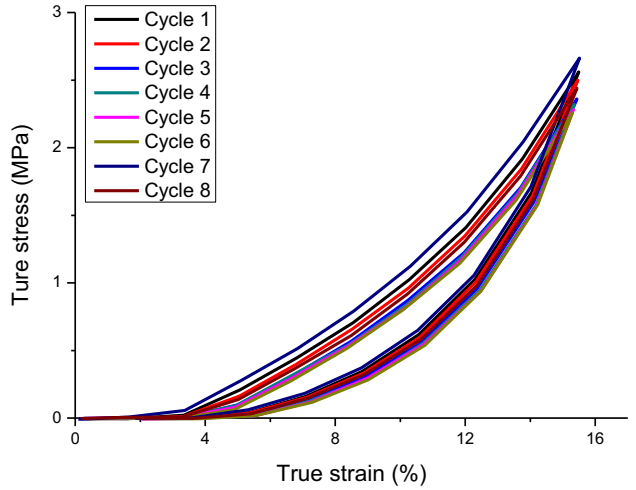

Fig. 6 – A cyclic stress–strain curve of a PGS/PLA core/shell fibrous mesh spun at a core feed flow rate of 0.3 ml/h and a shell feed flow rate of 0.9 ml/h at 12 kV.

PGS/PLLA fibres soaked in the culture medium, as well as in the two control groups, as shown in Fig. 8. Quantitative LDH measurements, shown in Fig. 9, demonstrated that the cytocompatibility of the PGS/PLA fibrous materials was of the same standard as the two control groups, with no significant differences in cell death between cultures containing the PGS/PLA fibrous meshes and material-free control cultures.

3.7. *Viability and function of hESC-derived cardiomyocytes*

To assess the viability of beating ESC-CMs, beating clusters were directly placed in the medium that had been soaked with PGS/PLLA mesh specimens. Visual examination showed beating hESC-CM cardiomyocytes remained a healthy phenotype when cultured in the presence of the PGS/PLLA mesh (spun at a core feed flow rate of 0.3 ml/h and a shell feed flow rate of 0.9 ml/h, and treated at 130 °C for 3 days). hESC-CMs were maintained as spontaneously beating colonies for over 1 month until interrupted, with beating rates of hESC-CM clusters in the presence of PGS/PLLA comparable to a larger population on tissue culture plastic (Fig. 10). Values of beating rates for hESC-CM in the presence of PGS/PLLA at various time points lie within the range for hESC-CM in material-free medium, indicating that the PGS/PLLA materials are capable of supporting optimal functional activity of hESC-CM.

4. Summary

Non-linearly elastic biomaterials were successfully fabricated from a chemically cross-linked PGS elastomer and a thermoplastic PLLA, using the core/shell electrospinning technique. The optimal fabrication conditions were established for electrospinning, including the critical parameter for spinning, which is the ratio of the feed flow rate of the core solution to the shell solution which ranges from 1:3 to 1:4 (Table 3).

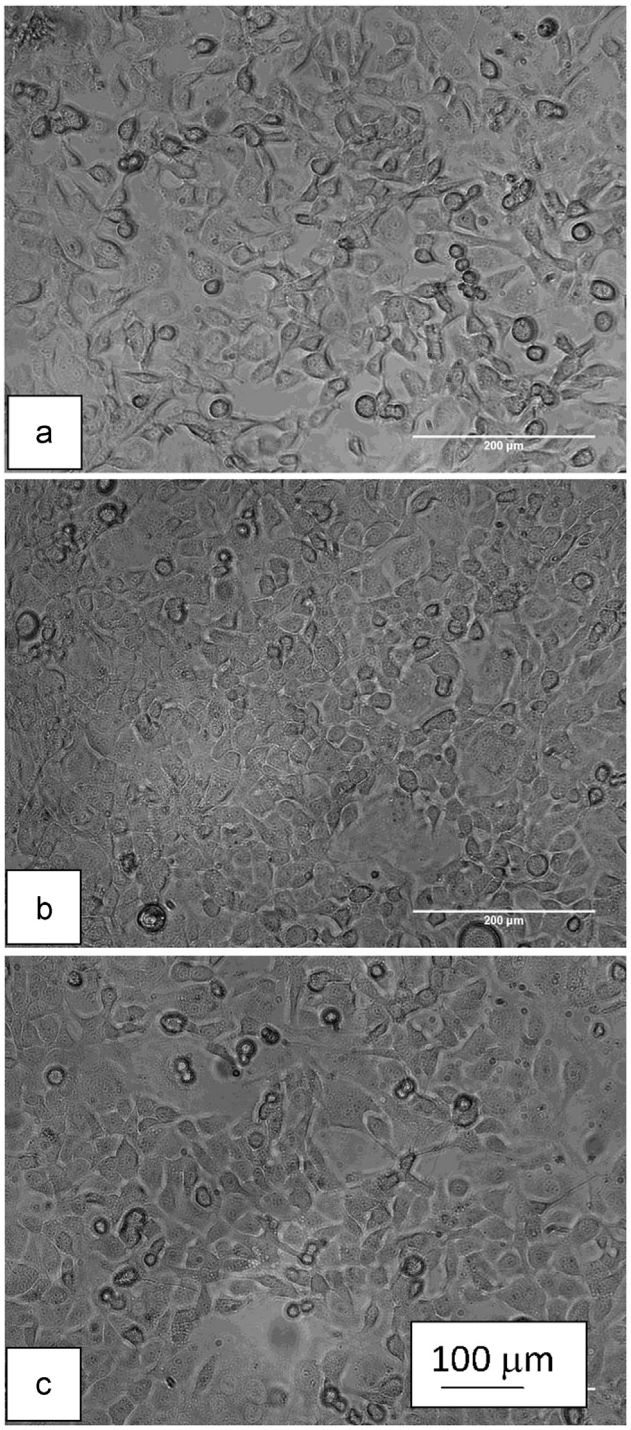

Fig. 7 – SNL cells cultured for five days in a material-free culture medium (negative control) (a), PGS/PLLA fibre mesh soaked with culture medium, produced from spinning at a core feed flow rate of 0.3 ml/h and a shell feed flow rate of 0.9 ml/h at 12 kV followed by PGS cross-linking at 130 °C for three days (b), and PLLA fibre mesh soaked with culture medium and used as a positive control (c).

Under optimal conditions, the electro-spun PGS/PLLA core/shell fibrous materials demonstrated muscle-like mechanical properties with J-shaped, elastic stress–strain curves, and the UTS, rupture elongation and stiffness constant of the

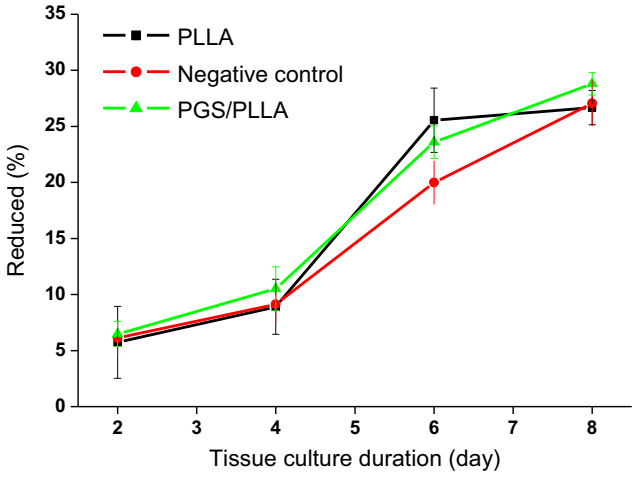

Fig. 8 – SNL cell proliferation kinetics measured by the AlamarBlue™ technique. The initial plating density was 2000 cells per well in a 48-well plate ($n=5$). Overall, there were no significant differences between any two of the three groups that were analysed ($p>0.05$). The PGS/PLLA fibre mesh was spun at a core feed flow rate of 0.3 ml/h and a shell feed flow rate of 0.9 ml/h at 12 kV followed by PGS cross-linking at 130 °C for three days.

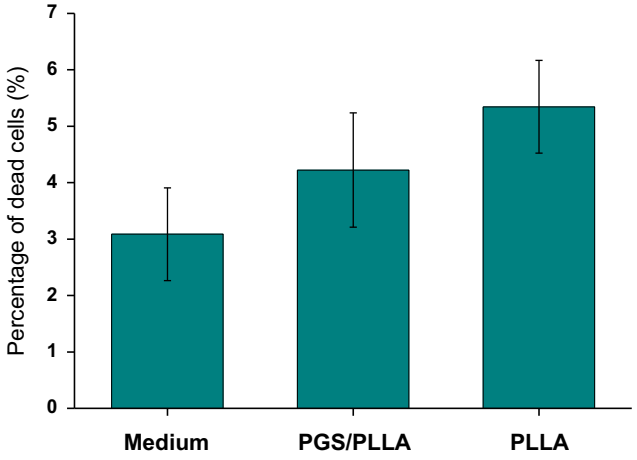

Fig. 9 – Cytotoxicity of PGS/PLLA core/shell spun materials, detected by measuring the release of lactate dehydrogenase (LDH) from the cells after four days of cultivation ($n=5$). No significant differences existed between any two of the three groups ($p>0.05$). The PGS/PLLA fibre mesh was spun at a core feed flow rate of 0.3 ml/h, and a shell feed flow rate of 0.9 ml/h at 12 kV followed by PGS cross-linking at 130 °C for three days.

PGS/PLLA fibrous meshes were 1±0.2 MPa, 25±3% and 18±2, respectively; these findings are as good as those observed in studies of heart muscular tissues. *In vitro* evaluations demonstrated that the PGS/PLLA core/shell fibres are excellent biocompatible materials. Finally, the large number of variables in the core/shell electrospinning process provides a wide range of possible mechanical properties and degradation kinetics, which could broadly be applied to the engineering of many soft tissues, such as tendon, ligament, cardiac

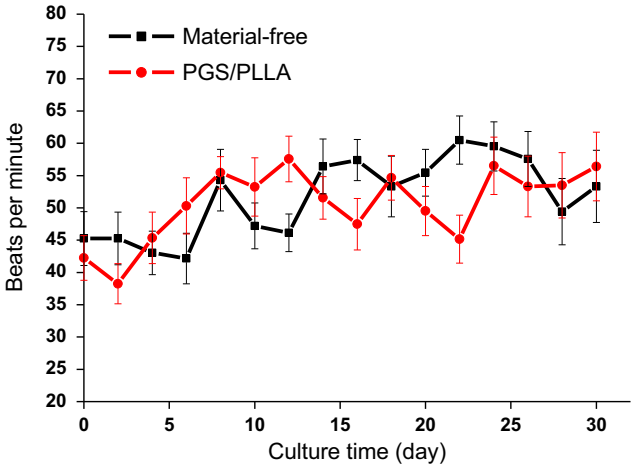

Fig. 10 – Average beating rate of cardiomyocytes in basal media compared with cardiomyocytes cultured in the presence of PGS/PLLA core–shell spun fibrous sheet.

muscle and lung epithelium. Further research will focus on the expansion of the mechanical and degradation profiles of this material system, as well as *in vivo* clinical applications.

Acknowledgements

We would like to thank Ms Karla Contreras for her technical assistance in the conduction of the tissue culture work at Monash University. The project was funded by Australian Research Council (DP130101384).

REFERENCES

Anseth, K.S., Shastri, V.R., Langer, R., 1999. Photopolymerizable degradable polyanhydrides with osteocompatibility. Nature Biotechnology 17, 156–159.

Bellingham, C.M., Lillie, M.A., Gosline, J.M., Wright, G.M., Starcher, B.C., Bailey, A.J., Woodhouse, K.A., Keeley, F.W., 2003. Recombinant human elastin polypeptides self-assemble into biomaterials with elastin-like properties. Biopolymers 70, 445–455.

Bettinger, C.J., Weinberg, E.J., Kulig, K.M., Vacanti, J.P., Wang, Y., Borenstein, J.T., Langer, R., 2006. Three-dimensional microfluidic tissue-engineering scaffolds using a flexible biodegradable polymer. Advanced Materials 18, 165–169.

Bognitzki, M., Czado, W., Frese, T., Schaper, A., Hellwig, M., Steinhart, M., Greiner, A., Wendorff, J.H., 2001. Nanostructured fibers via electrospinning. Advanced Materials 13, 70–72.

Caruso, R.A., S.J.H., Greiner, A., 2001. Titanium dioxide tibes from sol–gel coating of electrospun polymer fibers. Advanced Materials 13, 1577–1579.

Chen, Q.-Z., Bismarck, A., Hansen, U., Junaid, S., Tran, M.Q., Harding, S.E., Ali, N.N., Boccaccini, A.R., 2008a. Characterisation of a soft elastomer poly(glycerol sebacate) designed to match the mechanical properties of myocardial tissue. Biomaterials 29, 47–57.

Chen, Q.-Z., Ishii, H., Thouas, G.A., Lyon, A.R., Wright, J.S., Blaker, J.J., Chrzanowski, W., Boccaccini, A.R., Ali, N.N., Knowles, J.C., Harding, S.E., 2010a. An elastomeric patch

derived from poly(glycerol sebacate) for delivery of embryonic stem cells to the heart. Biomaterials 31, 3885–3893.
Chen, Q.-Z., Li, Y., Jin, L.-Y., Quinn, J.M.W., Komesaroff, P.A., 2010b. A new sol–gel process for producing Na_2O-containing bioactive glass ceramics. Acta Biomaterialia 6, 4143–4153.
Chen, Q., Liang, S., Thouas, G.A., 2013. Elastomeric biomaterials for tissue engineering. Progress in Polymer Science 38, 584–671.
Chen, Q.Z., Harding, S.E., Ali, N.N., Lyon, A.R., Boccaccini, A.R., 2008b. Biomaterials in cardiac tissue engineering: Ten years of research survey. Materials Science and Engineering: R, 59; 1–37.
Chen, Q.Z., Ishii, H., Thouas, G.A., Lyon, A.R., Wright, J.S., Blaker, J.J., Chrzanowski, W., Boccaccini, A.R., Ali, N.N., Knowles, J.C., Harding, S.E., 2010c. An elastomeric patch derived from poly (glycerol sebacate) for delivery of embryonic stem cells to the heart. Biomaterials 31, 3885–3893.
Chen, Q.Z., Jin, L.Y., Cook, W.D., Mohn, D., Lagerqvist, E.L., Elliott, D.A., Haynes, J.M., Boyd, N., Stark, W.J., Pouton, C.W., Stanley, E.G., Elefanty, A.G., 2010d. Elastomeric nanocomposites as cell delivery vehicles and cardiac support devices. Soft Matter 6, 4715–4726.
Chen, Q.Z., Liang, S.L., Thouas, G.A., 2011. Synthesis and characterisation of poly(glycerol sebacate)-co-lactic acid as surgical sealants. Soft Matter 7, 6484–6492.
Fester, A., Samet, P., 1974. Passive elasticity of human left ventricle. The 'parallel elastic element'. Circulation 50, 609–618.
Flory, P.J., 1953. Principles of Polymer Chemistry. Cornell Univ. Pr, Ithaca.
Freed, L.E., Engelmayr, G.C., Borenstein, J.T., Moutos, F.T., Guilak, F., 2009. Advanced material strategies for tissue engineering scaffolds. Advanced Materials 21, 3410–3418.
Freed, L.E., Guilak, F., Guo, X.E., Gray, M.L., Tranquillo, R., Holmes, J.W., Radisic, M., Sefton, M.V., Kaplan, D., Vunjak-Novakovic, G., 2006. Advanced tools for tissue engineering: scaffolds, bioreactors, and signaling. Tissue Engineering 12, 3285–3305.
Fung, Y.C.B., 1967. Elasticity of soft tissues in simple elongation. American Journal of Physiology, 1532–1544.
Gosline, J., Lillie, M., Carrington, E., Guerette, P., Ortlepp, C., Savage, K., 2002. Elastic proteins: biological roles and mechanical properties. Philosophical Transactions of the Royal Society of London Series B – Biological Sciences 357, 121–132.
Haut, R.C., Little, R.W., 1972. A constitutive equation for collagen fibers. Journal of Biomechanics 5 (423–424), 425–430 (IN421).
Jiang, H.L., Hu, Y.Q., Zhao, P.C., Li, Y., Zhu, K.J., 2006. Modulation of protein release from biodegradable core–shell structured fibers prepared by coaxial electrospinning. Journal of Biomedical Materials Research Part B 79B, 50–57.
Li, D., Xia, Y., 2004. Electrospinning of nanofibers: reinventing the wheel?. Advanced Materials 16, 1151–1170.
Li, Y., Cook, W.D., Moorhoff, C., Huang, W.-C., Chen, Q.-Z., 2013. Synthesis, characterization and properties of biocompatible poly(glycerol sebacate) pre-polymer and gel. Polymer International 62, 534–547.
Liang, S.-L., Cook, W.D., Thouas, G.A., Chen, Q.-Z., 2010. The mechanical characteristics and in vitro biocompatibility of poly(glycerol sebacate)-Bioglass® elastomeric composites. Biomaterials 31, 8516–8529.
Liang, S., Cook, W.D., Chen, Q., 2012. Physical characterization of poly(glycerol sebacate)/Bioglass® composites. Polymer International 61, 17–22.
Lv, S., Dudek, D.M., Cao, Y., Balamurali, M.M., Gosline, J., Li, H.B., 2010. Designed biomaterials to mimic the mechanical properties of muscles. Nature 465, 69–73.
Malberg, S., Basalp, D., Finne-Wistrand, A., Albertsson, A.C., 2010. Bio-safe synthesis of linear and branched PLLA. Journal of Polymer Science Part A – Polymer Chemistry 48, 1214–1219.
Mirsky, I., 1976. Assessment of passive elastic stiffness of cardiac-muscle -methematical concepts, physiologic and clinical considerations, directions of future research. Progress in Cardiovascular Diseases 18, 277–308.
Mirsky, I., Cohn, P.F., Levine, J.A., Gorlin, R., Herman, M.V., Kreulen, T.H., Sonnenbl, Eh., 1974. Assessment of left-ventricular stiffness in primary myocardial-disease and coronary-artery disease. Circulation 50, 128–136.
Mirsky, I., Parmley, W.W., 1973. Assessment of passive elastic stiffness for isolated heart-muscle and intact heart. Circulation Research 33, 233–243.
Ou, K.-L., Chen, C.-S., Lin, L.-H., Lu, J.-C., Shu, Y.-C., Tseng, W.-C., Yang, J.-C., Lee, S.-Y., Chen, C.-C., 2011. Membranes of epitaxial-like packed, super aligned electrospun micron hollow poly(l-lactic acid) (PLLA) fibers. European Polymer Journal 47, 882–892.
Ravichandran, R., Venugopal, J.R., Sundarrajan, S., Mukherjee, S., Ramakrishna, S., 2011. Poly(glycerol sebacate)/gelatin core/shell fibrous structure for regeneration of myocardial infarction. Tissue Engineering Part A 17, 1363–1373.
Seal, B.L., Otero, T.C., Panitch, A., 2001. Polymeric biomaterials for tissue and organ regeneration. Materials Science and Engineering: R: Reports 34, 147–230.
Stromber, D.D., Wiederhi, C.A., 1969. Viscoelastic description of a collagenous tissue in simple elongation. Journal of Applied Physiology 26, 857–862.
Stuckey, D.J., Ishii, H., Chen, Q.Z., Boccaccini, A.R., Hansen, U., Carr, C.A., Roether, J.A., Jawad, H., Tyler, D.J., Ali, N.N., Clarke, K., Harding, S.E., 2010. Magnetic resonance imaging evaluation of remodeling by cardiac elastomeric tissue scaffold biomaterials in a rat model of myocardial infarction. Tissue Engineering Part A 16, 3395–3402.
Sun, Z.-J., Wu, L., Huang, W., Zhang, X.-L., Lu, X.-L., Zheng, Y.-F., Yang, B.-F., Dong, D.-L., 2009. The influence of lactic on the properties of poly (glycerol–sebacate–lactic acid). Materials Science and Engineering: C 29, 178–182.
Sun, Z.C., Zussman, E., Yarin, A.L., Wendorff, J.H., Greiner, A., 2003. Compound core–shell polymer nanofibers by co-electrospinning. Advanced Materials 15, 1929.
Szczesny, S.E., Peloquin, J.M., Cortes, D.H., Kadlowec, J.A., Soslowsky, L.J., Elliott, D.M., 2012. Biaxial tensile testing and constitutive modeling of human supraspinatus tendon. Journal of Biomechanical Engineering 134 (021004-021004).
Takaoka, H., Esposito, G., Mao, L., Suga, H., Rockman, H.A., 2002. Heart size-independent analysis of myocardial function in murine pressure overload hypertrophy. American Journal of Physiology – Heart and Circulatory Physiology 282, H2190–H2197.
Taylor, G.R., Darin, S.R., 1955. The tensile strength of elastomers. Journal of Polymer Science 17, 511–525.
Tsuji, H., Nakano, M., Hashimoto, M., Takashima, K., Katsura, S., Mizuno, A., 2006. Electrospinning of poly(lactic acid) stereocomplex nanofibers. Biomacromolecules 7, 3316–3320.
Veress, A.I., Gullberg, G.T., Weiss, J.A., 2005. Measurement of strain in the left ventricle during diastole with cine-MRI and deformable image registration. Journal of Biomechanical Engineering – Transactions of the ASME 127, 1195–1207.
Wang, Y., Ameer, G.A., Sheppard, B.J., Langer, R., 2002. A tough biodegradable elastomer. Nature Biotechnology 20, 602–606.
Yi, F., Lavan, D.A., 2008. Poly(glycerol sebacate) nanofiber scaffolds by core/shell electrospinning. Macromolecular Bioscience 8, 803–806.
Zhang, Y.Z., Huang, Z.M., Xu, X.J., Lim, C.T., Ramakrishna, S., 2004. Preparation of core–shell structured PCL-r-gelatin Bi-component nanofibers by coaxial electrospinning. Chemical Materials 16, 3406–3409.